Title	Transmural transverse stiffness estimation in vascular shear wave imaging: A simulation and phantom study
Author(s)	GUO, Y; Lo, HY; Lee, W
Citation	Applied Physics Letters, 2017, v. 110, p. 193701:1-193701:5
Issued Date	2017
URL	http://hdl.handle.net/10722/240921
Rights	Applied Physics Letters. Copyright © American Institute of Physics.; After publication: Copyright (2017) American Institute of Physics. This article may be downloaded for personal use only. Any other use requires prior permission of the author and the American Institute of Physics. The following article appeared in (Applied Physics Letters, 2017, v. 110, p. 193701:1-193701:5) and may be found at (http://dx.doi.org/10.1063/1.4983290).; This work is licensed under a Creative Commons Attribution-NonCommercial-NoDerivatives 4.0 International License.

Transmural transverse stiffness estimation in vascular shear wave imaging: A simulation and phantom study

Yuexin Guo,[1] Ho Yuen Lo,[1,2] and Wei-Ning Lee[1,2,a)]
[1]*Department of Electrical and Electronic Engineering, The University of Hong Kong, Hong Kong*
[2]*Medical Engineering Programme, The University of Hong Kong, Hong Kong*

(Received 16 December 2016; accepted 28 April 2017; published online 9 May 2017)

Shear wave imaging has emerged as a potential non-invasive technique for the quantitative assessment of the arterial shear modulus. Nonetheless, the arterial elasticity estimation in the transverse direction has been overlooked compared with the longitudinal direction, and the estimated transmural stiffness has rarely been evaluated. Accurate depiction of the transverse stiffness across the thin arterial wall warrants comprehensive characterization in both normal and pathological conditions. This study estimated the transmural arterial shear modulus in both the longitudinal (μ_{Long}) and transverse directions (μ_{Trans}) using group (c_T) and phase velocities (c_{ph}) in finite element models and hollow cylindrical tissue-mimicking phantoms with various shape factors. The results were validated against mechanical testing. Zero-order antisymmetric Lamb wave and circumferential Lamb type wave models were considered in the longitudinal and transverse directions of the thin-walled hollow cylinder, respectively. The results derived from the model with the thin plate assumption confirmed that c_T underestimated μ_{Long} and μ_{Trans}. Unlike the c_{ph}-based μ_{Long} estimates that were in excellent agreement with measured values, the c_{ph}-based μ_{Trans} estimates were found to be comparable to c_{ph}-based μ_{Long} at the inner wall but increased radially outward. Transmural μ_{Trans} estimation using c_{ph} was demonstrated to be feasible for thin-walled hollow cylinders but necessitated careful account of the wall geometry, in particular the shape factor. *Published by AIP Publishing.*
[http://dx.doi.org/10.1063/1.4983290]

Arterial stiffness has been recognized as an important independent predictor of various cardiovascular diseases, such as hypertension, stroke, and heart failure.[1] Decreased arterial compliance degrades the capacity of the artery.[2,3] Excessive stiffness may also damage the peripheral target organs owing to the overload pressure pulsatility.[4,5] A variety of risk factors and biological processes that exacerbate cardiovascular diseases also influence arterial stiffness.[6,7] Pronounced local changes in arterial wall stiffness are found in pathological conditions, such as atherosclerosis and aortic aneurysm,[8] rendering it imperative to assess transmural arterial stiffness.

The noninvasive measurement of global or regional arterial stiffness is performed using several methods,[9] predominantly pulse wave velocity (PWV).[10] The pulse wave is generated by the systolic pressure during the blood ejection through the aorta. The Young's modulus of the arterial wall is linked to PWV via the Moens-Korteweg equation.[2] Imaging regional PWV in the carotid artery and the aorta has been achieved with magnetic resonance imaging (MRI)[11–13] and ultrasound.[14–16] However, the intrinsic pulse wave occurs during the ejection phase of the cardiac cycle. Because of its low temporal frequency, PWV is not ideal for the assessment of the arterial stiffness variation over the entire cardiac cycle.

Unlike PWV-based imaging methods, shear wave imaging (SWI)[17] generates, captures, and analyzes shear waves, whose propagation speed (c_T) has a simple direct relationship with the shear modulus (μ) of homogeneous, isotropic, linear elastic bulk soft tissues with density of ρ as follows:

$$\mu = \rho c_T^2, \tag{1}$$

where c_T is the group velocity of the generated bulk shear wave. SWI has been made commercially available for characterizing *in vivo* bulk soft tissues, including the breast[18] and the liver,[19,20] but has not yet been made available for arteries.

Compared with PWV-based stiffness estimates available only at specific cardiac phases, the SWI-based arterial shear modulus could theoretically be obtained at an arbitrary time point within the cardiac cycle. Unlike the generated shear wave propagating in bulk soft tissues, the induced elastic wave in the artery, i.e., a hollow cylindrical structure, falls in the guided wave mode. The wave reflections at the interfaces tend to confine the wave energy within the layered structure, which acts as a guide for the wave. Multiple propagation paths form specific interference patterns that are related to the elasticity, density, and thickness of the layered material and the wavelength of the guided wave. Therefore, dispersion, which refers to the phenomenon that each frequency component of the guided wave travels at a different velocity, occurs even in a purely elastic thin medium. For guided waves propagating in the longitudinal direction of a hollow cylinder, a thin plate assumption has been proven valid.[21] A zero-order antisymmetric Lamb wave model has been proposed[22] as follows:

a)Electronic mail: wnlee@eee.hku.hk

$$4k_L^3\beta\cosh(k_Lh/2)\sinh(\beta h/2)-\left(k_s^2-2k_L^2\right)^2\sinh(k_Lh/2)\times\cosh(\beta h/2)=k_s^4\cosh(k_Lh/2)\cosh(\beta h/2), \quad (2)$$

where h is the thickness of the arterial wall, $k_L=\omega/c_{ph}$ is the Lamb wave number, ω is the angular frequency, c_{ph} is the frequency-dependent Lamb wave phase velocity, $\beta=\sqrt{k_L^2-k_s^2}$, and $k_s=\omega\sqrt{\rho/\mu}$. Because both k_s and β are functions of μ, the latter can be derived by fitting the measured c_{ph} to the theoretical model.

Most studies have quantified the arterial shear modulus in the longitudinal direction (μ_{Long}).[22–24] However, the artery is mechanically anisotropic because of its complex and layered wall structure;[25–27] therefore, assessing arterial shear modulus in multiple directions is indispensable. To estimate the transverse arterial shear modulus (μ_{Trans}) using SWI, the circumferentially propagating guided wave, which has been extensively studied in non-destructive testing (NDT),[28–31] shall be investigated. This type of wave with displacement along the radial direction is referred to as a circumferential Lamb type wave (CLT-wave). The angular wave number k_{ang}, which is a unique physical phenomenon of circumferentially propagating waves, is defined for modeling CLT-waves[29] as follows:

$$k_{ang}=\omega^r/\left(c_{ph}^r\times r\right), \quad (3)$$

where ω^r and c_{ph}^r are the angular frequency and linear phase velocity at a radial position (r), respectively. The wave fronts along the same radial line exhibit the same angular velocity in CLT-waves. Therefore, the propagation of CLT-waves can be represented as the rotation of the radial line. The linear phase velocity thereby increases radially outward. Numerical examples[29,30] have shown that CLT-waves depend on the shape factor p, which is defined as

$$p=r_{in}/r_{out}, \quad (4)$$

where r_{in} and r_{out} are the inner and outer radii, respectively. When p approaches unity, the thin circular annulus can be approximated as a thin-layered structure. For the aorta and carotid artery, the shape factor p is typically larger than 0.8. In such cases, Eq. (2) may act as a valid model for the CLT-wave. However, for the estimation of the transverse arterial shear modulus (μ_{Trans}), only c_T-based estimates based on the bulk medium assumption have been studied.[25–27,32,33] One recent study[34] demonstrated the feasibility of using the c_{ph}-based technique with Lamb wave assumption for arterial stiffness estimation in finite element models (FEMs) and phantoms. However, these studies reported arterial stiffness either at a specific radial position, e.g., mid-wall,[32,34] or averaged across the wall,[25,26,33] without considering the transmural variation of linear velocity. How the arterial curvature in the transverse direction guides the wave propagation and the transmural stiffness estimation remains unknown.

Therefore, we investigated the feasibility of estimating transmural μ_{trans} using c_{ph} based on the assumption of a thin-plate structure. Using simulations and controlled artery-mimicking phantoms with various geometric parameters, we compared the biplanar SWI-estimated stiffnesses using c_T and c_{ph}.

In this study, guided wave propagation in homogeneous, isotropic, and linear elastic hollow cylinders [Fig. 1(a)] was investigated using COMSOL Multiphysics 5.0 (Comsol Inc. Burlington, MA, USA). Five three-dimensional (3D) FEMs of cylinders whose radii ranged from 5 to 13 mm (Table I) were simulated and interfaced with water. The radii were chosen to correspond with average dimensions of the human aorta.[35] The Young's modulus, Poisson's ratio, and density of the simulated cylinders were 100 kPa, 0.4995, and 1000 kg/m^3, respectively. A Gaussian impulse stimulus [Fig. 1(b)] with an amplitude of 1 μm and a duration of 100 μs was applied radially within a cylindrical region of $\pi\times1^2\times2$ mm^3 throughout the entire thickness of the upper wall [Fig. 1(a)]. The guided wave propagations at five radial positions from the inner to the outer boundaries at an increment of 0.05 mm in two orthogonal directions were exported [Figs. 1(c) and 1(d)].

Five homogeneous and isotropic artery-mimicking phantoms were made of polyvinyl alcohol (PVA) powders (Sigma-Aldrich® M_w 89 000–98 000, 99+% hydrolyzed), which is a suitable soft tissue mimicking material for medical ultrasound imaging.[36–38] The geometric parameters of the artery-mimicking phantoms matched those in the simulations (Table I). The solution was composed of 88% de-ionized water, fully dissolved 10% PVA, 1% SiO_2, and 1% potassium sorbate by weight. The room temperature PVA solution was poured into 3D printed molds. Each PVA phantom went through five freeze/thaw (F/T) cycles (12 h at −23 °C and 12 h at room temperature) and its Young's modulus was measured from the stress-strain curve obtained from standard mechanical testing (see supplementary material).[39]

A Vantage 256 system (Verasonics Inc., Kirkland, WA) with an L11–4v probe (128 elements, Verasonics Inc.,

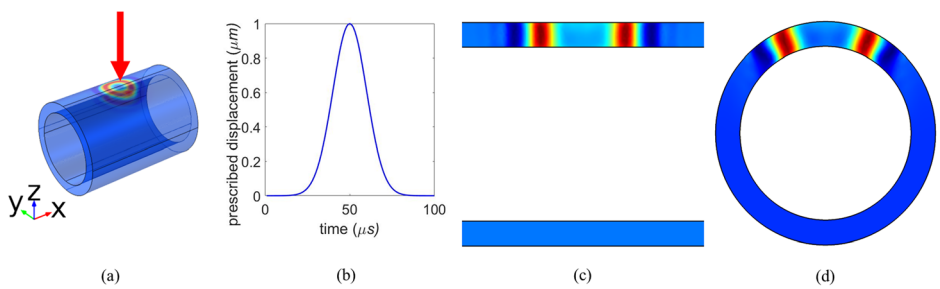

FIG. 1. Finite element model of case 2 (Table I): (a) a homogeneous, isotropic, and linear elastic hollow cylinder interfaced with water is excited by (b) a prescribed Gaussian impulse for guided wave generation. The location and direction of the excitation are indicated by the red arrow. (c) and (d) are the resulting guided waves in the longitudinal and transverse directions at 700 μs after the excitation, respectively. The displacement is normalized to [−1, 1] for visualization.

TABLE I. Finite element models (FEMs) and artery-mimicking phantom properties.

	FEM		Artery-mimicking phantom		
Case	Inner radius R_{in} (mm)	Outer radius R_{out} (mm)	Inner radius R_{in} (mm)	Outer radius R_{out} (mm)	Shear modulus μ (kPa)[a]
1	5	7	4.7	6.7	17.17
2	7	9	6.7	8.4	16.67
3	9	11	8.5	10.3	16.95
4	11	13	10.6	12.4	18.56
5	13	15	13.8	15.8	20.21

[a]Shear modulus μ was obtained by mechanical testing (see supplementary material).

Kirkland, WA) was used to remotely induce guided waves by a single ultrasonic focused beam (5 MHz; F-number = 1; 100 μs) in the upper wall of each artery-mimicking phantom (Fig. 2). Coherent plane wave compounding[40] with three tilted angles (−4°, 0°, and 4°) at the center frequency of 8.9 MHz was employed to achieve a frame rate higher than 4000 Hz without severely sacrificing image resolution and sonographic signal-to-noise ratio (SNR). The in-phase and quadrature (IQ) data were acquired and stored for offline analysis. The ultrasound probe was mounted on a rotation stage URS 100 (Newport Inc., Irvine, California) to perform biplanar vascular SWI measurements. The measurement was repeated six times at the same location within each phantom in each direction.

The stored IQ data were compounded, and each successive pair of compounded frames was cross-correlated to yield an acoustic radiation force (ARF)-induced tissue velocity (i.e., guided wave amplitude) map [Figs. 2(a) and 2(e)]. For CLT-waves, each corresponding tissue velocity map was warped from an annulus shape to a rectangular slab (see supplementary material). A spatiotemporal map at each wall depth in either the longitudinal [Fig. 2(b)] or the warped transverse direction [Fig. 2(f)] was obtained to estimate the guided wave propagation speed (c_T and c_{ph}) within the region of interest (ROI) (4 ms × 13.5 mm) in all cases. The size of the ROI was found to be temporal-length dependent and was optimized by balancing the trade-off between resolution and accuracy. To estimate c_T, the maximum guided wave amplitude in the first frame was tracked using 1 D cross correlation[41] with a kernel size of approximately 3 mm throughout each spatiotemporal map. The slope of the linearly fitted line represented c_T.

For c_{ph} estimation, the spatiotemporal map was first transformed into the wavenumber-frequency domain (i.e., k-space) by discrete 2D fast Fourier transform [Figs. 2(c) and 2(g)].[22,23] To remove the background noise, the signals lower than 10% of the maximum intensity of the entire k-space data were nulled.[24] Then, a high-pass filter with a cutoff frequency of 50 Hz was applied in both the temporal and spatial domains to remove the high intensity noise at low frequencies. The maximum intensity at a specific frequency f was subsequently identified, corresponding to a wave number k_L^f. The phase velocity at f was calculated as

$$c_{ph}^f = 2\pi f / k_L^f. \tag{5}$$

To accurately estimate the shear modulus, Eq. (2) was fit to the high frequency component (>500 Hz) of the dispersion curve [Figs. 2(d) and 2(h)].

The simulated phase velocity analysis confirmed that wave dispersion occurred in both the longitudinal and transverse directions of a purely elastic thin-walled hollow cylinder (Fig. 3). The simulation results [Fig. 3 (top row)] show that the estimated μ_{Long} was nearly constant using either c_T(13.53±0.65 kPa) or c_{ph}(35.20±0.35 kPa). Compared with the actual value (μ = 33.3 kPa), the group velocity significantly underestimated μ_{Long}, while c_{ph} provided a much more reliable estimation with absolute and relative errors being 1.90±0.57 kPa and 5.7±1.7%, respectively; these results are consistent with a recent study.[24] Therefore, the c_{ph}-based μ_{long} estimates served as a reference for the estimation of μ_{trans} in the thin-walled hollow cylinders. The c_{ph}-based μ_{trans} estimates were found to be comparable to c_{ph}-based μ_{long} estimates at the inner wall but increased radially outward.

The artery-mimicking phantom results [Fig. 3(bottom row)] were in excellent agreement with those from the simulations. The c_T–based approach underestimated μ_{Long}, whereas the estimated μ_{Long} based on c_{ph} agreed well with the mechanical testing measurements throughout the wall, with an absolute error of 0.53±0.36 kPa and a relative error of

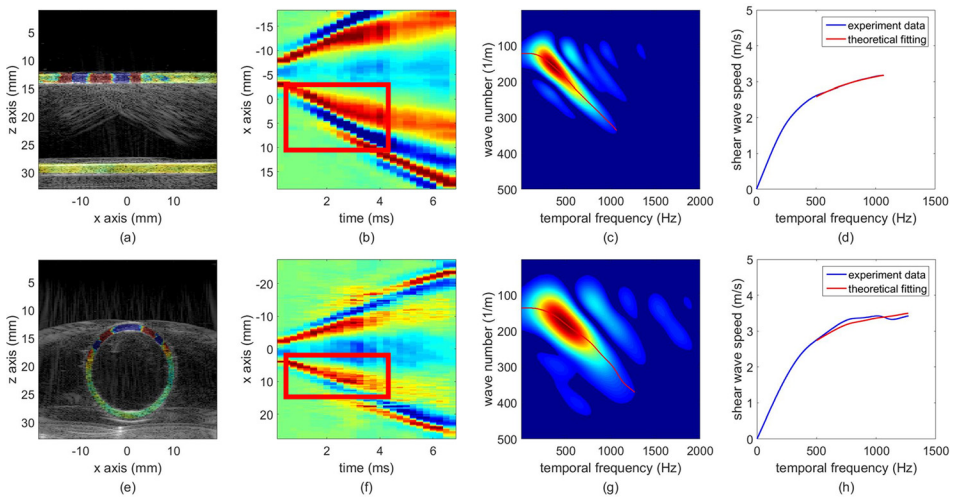

FIG. 2. Guided wave propagation and phase velocity analysis in the case 2 artery-mimicking phantom in the longitudinal (top) and transverse (bottom) directions: (a) and (e) B-mode images overlaid with estimated ARF-induced tissue velocities, which are displayed in the scale from −60 to 0 dB, at 1.5 ms; (b) and (f) spatiotemporal maps, in which the red boxes indicate the ROIs for wave analysis; (c) and (g) k-space data of (b) and (f); and (d) and (h) experimental dispersion curves fit to the zero-order antisymmetric Lamb wave model.

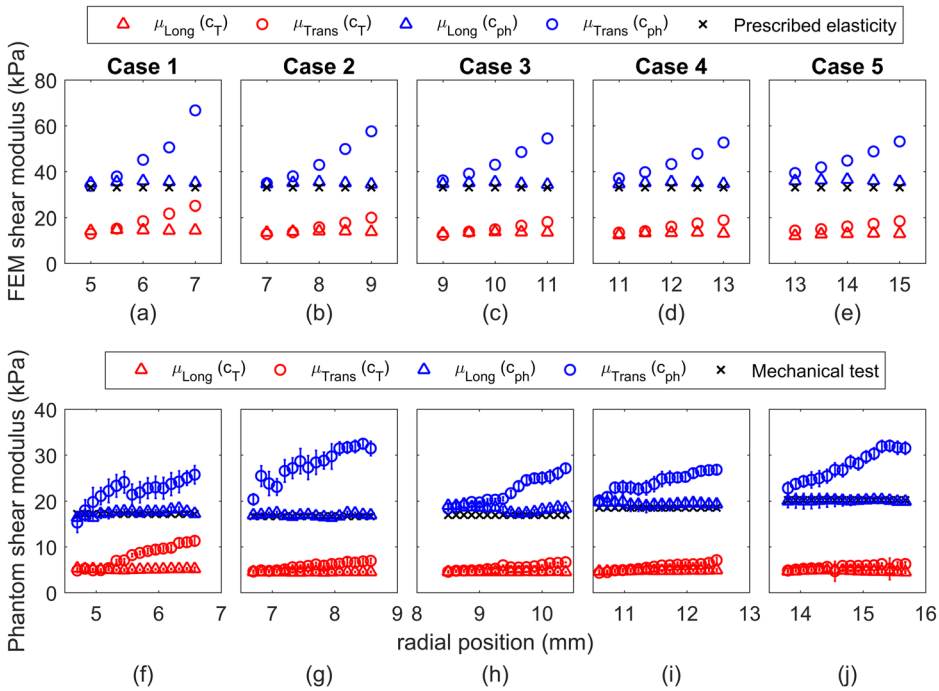

FIG. 3. The estimated shear moduli across the wall based on c_T and c_{ph} in the longitudinal (μ_{Long}) and transverse (μ_{Tong}) directions from five FEMs (top) and five artery-mimicking phantoms (bottom).

3.10±3.39%. The estimated μ_{Trans} based on c_{ph} was accurate at the inner wall (absolute error: 1.54±0.75 kPa; relative error: 9±4.38%) and also showed a significant outward radial increase. In both simulations and phantom experiments, shear moduli were greatly underestimated using c_T but were accurately estimated based on c_{ph} as validated by mechanical testing.[24,42]

Previous studies of the circumferential wave propagation within a hollow cylindrical structure were mainly based on the bulk medium assumption,[25–27,32,33] which was found valid when the thickness was comparable to the wavelength of the generated shear wave (~5 mm).[32] Negligence of both the dispersion in the thin-plate structure and the transmural variation of linear velocity may have led to the discrepancy between the estimated and actual values.[25,32] In contrast, our study took into account the aforementioned physical phenomena for μ_{Trans} estimation.

Both simulation and artery-mimicking phantom results demonstrated that the complex propagation of guided waves in hollow cylinders with high shape factor (>0.7) in the warped transverse direction could be approximated as a zero-order anti-symmetric Lamb wave in a thin-plate structure composed of a homogenous, isotropic, and linear elastic material immersed in water. Previous studies[25,32] that investigated μ_{Trans} were based on the assumption of shear wave propagation within an infinite medium; only the c_T-based approach was implemented, and the reported results showed significant discrepancies between the measured and actual values.[25,32] To address this issue, our study investigated the use of c_{ph} for the estimation of μ_{Trans} by vascular SWI and systematically explored the influence of the geometry of the thin-walled hollow cylinder on stiffness estimation in both simulations and artery-mimicking phantoms. The outward radial increase of the estimated μ_{Trans} was consistent with the reported radial increase of the linear phase velocity in NDT studies.[28–30] The transmural variation of μ_{Trans} was less pronounced with larger shape factors. Therefore, the estimated μ_{Trans} depended on the radial position and required taking into account the geometry with the thin-plate assumption.

With the artery-mimicking phantoms, poorer estimation of μ_{Trans} than μ_{Long} was found, possibly owing to the uncertainty of identifying the inner boundaries. To accurately track the guided wave propagation in the transverse direction, the transmural tracking line had to reside in the cross-section of the artery-mimicking phantom. If the assumed inner circular propagation path did not exactly coincide with the actual inner boundary of the artery-mimicking phantom, an overestimation of r_{in} might have resulted. The low quality of the B-mode image acquired by ultrafast imaging techniques may also have led to poor boundary delineation and thus the overestimation of r_{in} and μ_{Trans}. A possible solution would be including an additional conventional imaging mode, e.g., single focus, in the SWI examinations to acquire a high-quality B mode image. When the CLT-wave arrived at 3 and 9 o'clock, the vibration direction became dominantly lateral, which was not tracked and thus not displayed. As shown in Fig. 2(f), the wave front became noisy and disturbed at around 3.5 ms when the waves arrived at 3 and 9 o'clock, further degrading the performance of vascular SWI.

Several other challenges remain in c_{ph}-based vascular SWI. Although we showed that the zero-order anti-symmetric Lamb wave model could approximate the CLT-wave propagation near the inner surface, a closed-form expression independent of the radial position is preferred. A solution using mode eigenfunction expansion with heavy computational load has been proposed[30] but necessitates simplifications for clinical implementation. The assumed circumferential path does not necessarily hold in real scenarios because the cross-section of the artery might be elliptical or even irregular in pathological conditions. Therefore, a modified image warping method for tracking the circumferential guided wave propagation will be required. This study assumed the isotropic artery material, but the artery is actually anisotropic. The effect of the fiber and the multi-layer structure should be

taken into account. In an anisotropic material, μ_{Long} and μ_{Trans} may initially be distinct. The transmural variation of μ_{Trans} should also be corrected to accurately estimate the stiffness of each layer. Last, factors such as medium-coupling and time-varying luminal pressure were not considered in this study but are being investigated in a separate study.

This study substantiated the necessity and feasibility of c_{ph} estimation for accurately quantifying the transmural stiffness of a purely elastic, homogeneous, isotropic, and linear hollow cylindrical structure in the transverse and longitudinal directions and laid the foundation for *ex vivo* and *in vivo* experimental examinations.

See supplementary material for image warping and mechanical testing.

This study was supported by the National Natural Science Foundation of China (NSFC)/Research Grants Council (RGC) Joint Research Scheme (N_HKU713_15), University Development Fund, and Hong Kong Research Grants Council (ECS 739413E).

[1]P. Segers and P. Verdonck, in *Pan Vascular Medicine* (Springer, 2002), p. 116.
[2]W. Nichols, M. O'Rourke, and C. Vlachopoulos, *McDonald's Blood Flow in Arteries: Theoretical, Experimental and Clinical Principles* (CRC Press, 2011).
[3]M. F. O'Rourke, J. A. Staessen, C. Vlachopoulos, and D. Duprez, Am. J. Hypertens. **15**(5), 426 (2002).
[4]M. F. O'Rourke and M. E. Safar, Hypertension **46**(1), 200 (2005).
[5]S. J. Vermeersch, E. R. Rietzschel, M. L. De Buyzere, D. De Bacquer, G. De Backer, L. M. Van Bortel, T. C. Gillebert, P. R. Verdonck, and P. Segers, Physiol. Meas. **29**(11), 1267 (2008).
[6]R. A. Payne, I. B. Wilkinson, and D. J. Webb, Hypertension **55**(1), 9 (2010).
[7]C. M. McEniery, M. Spratt, M. Munnery, J. Yarnell, G. D. Lowe, A. Rumley, J. Gallacher, Y. Ben-Shlomo, J. R. Cockcroft, and I. B. Wilkinson, Hypertension **56**(1), 36 (2010).
[8]J. C. Lasheras, Annu. Rev. Fluid Mech. **39**, 293 (2007).
[9]C. L. De Korte, S. Fekkes, A. J. Nederveen, R. Manniesing, and H. H. G. Hansen, IEEE Transactions on Ultrasonics, Ferroelectrics, and Frequency Control **63**(10), 1613 (2016).
[10]J. D. Cameron, C. J. Bulpitt, E. S. Pinto, and C. Rajkumar, Diabetes Care **26**(7), 2133 (2003).
[11]J. M. Boese, M. Bock, S. O. Schoenberg, and L. R. Schad, Phys. Med. Biol. **45**(6), 1703 (2000).
[12]H.-Y. Yu, H.-H. Peng, J.-L. Wang, C.-Y. Wen, and W.-Y. I. Tseng, Magn. Reson. Med. **56**(4), 876 (2006).
[13]B. D. Bolster, E. Atalar, C. J. Hardy, and E. R. McVeigh, J. Magn. Reson. Imaging **8**(4), 878 (1998).
[14]P. J. Brands, J. M. Willigers, L. A. F. Ledoux, R. S. Reneman, and A. P. G. Hoeks, Ultrasound Med. Biol. **24**(9), 1325 (1998).
[15]J. Vappou, J. Luo, and E. E. Konofagou, Am. J. Hypertens. **23**(4), 393 (2010).
[16]J. Luo, R. X. Li, and E. E. Konofagou, IEEE Trans. Ultrason. Ferroelectr. Freq. Control **59**(1), 174 (2012).
[17]A. P. Sarvazyan, O. V. Rudenko, S. D. Swanson, J. B. Fowlkes, and S. Y. Emelianov, Ultrasound Med. Biol. **24**(9), 1419 (1998).
[18]M. Tanter, J. Bercoff, A. Athanasiou, T. Deffieux, J.-L. Gennisson, G. Montaldo, M. Muller, A. Tardivon, and M. Fink, Ultrasound Med. Biol. **34**(9), 1373 (2008).
[19]M. Muller, J.-L. Gennisson, T. Deffieux, M. Tanter, and M. Fink, Ultrasound Med. Biol. **35**(2), 219 (2009).
[20]L. Sandrin, B. Fourquet, J.-M. Hasquenoph, S. Yon, C. Fournier, F. Mal, C. Christidis, M. Ziol, B. Poulet, and F. Kazemi, Ultrasound Med. Biol. **29**(12), 1705 (2003).
[21]I. A. Viktorov, *Rayleigh and Lamb Waves: Physical Theory and Applications* (Plenum Press, 1970).
[22]M. Bernal, I. Nenadic, M. W. Urban, and J. F. Greenleaf, J. Acoust. Soc. Am. **129**(3), 1344 (2011).
[23]M. Couade, M. Pernot, C. Prada, E. Messas, J. Emmerich, P. Bruneval, A. Criton, M. Fink, and M. Tanter, Ultrasound Med. Biol. **36**(10), 1662 (2010).
[24]E. Maksuti, E. Widman, D. Larsson, M. W. Urban, M. Larsson, and A. Bjällmark, Ultrasound Med. Biol. **42**(1), 308 (2016).
[25]D. A. Shcherbakova, C. Papadacci, A. Swillens, A. Caenen, S. De Bock, V. Saey, K. Chiers, M. Tanter, S. E. Greenwald, and M. Pernot, Adv. Mech. Eng. **6**, 272586 (2014).
[26]D. Shcherbakova, A. Swillens, A. Caenen, S. De Bock, P. Segers, C. Papadacci, M. Tanter, M. Pernot, V. Saey, and K. Chiers, in *2013 IEEE International Ultrasonics Symposium (IUS)* (IEEE, 2013), p. 1545.
[27]M. W. Urban, I. Z. Nenadic, C. Pislaru, and J. F. Greenleaf, in *2013 IEEE International Ultrasonics Symposium (IUS)* (IEEE, 2013), p. 1765.
[28]J. Qu, Y. Berthelot, and Z. Li, in *Review of Progress in Quantitative Nondestructive Evaluation* (Springer, 1996), p. 169.
[29]G. Liu and J. Qu, ASME. J. Appl. Mech. **65**(2), 424–430 (1998).
[30]G. Liu and J. Qu, J. Acoust. Soc. Am. **104**(3), 1210 (1998).
[31]J. L. Rose, J. Pressure Vessel Technol. **124**(3), 273 (2002).
[32]H. H. G. Hansen, M. Pernot, S. Chatelin, M. Tanter, and C. L. de Korte, in *2015 IEEE International Ultrasonics Symposium (IUS)* (IEEE, 2015), p. 1.
[33]D. A. Shcherbakova, A. Caenen, A. Swillens, P. Segers, S. Chatelin, C. Papadacci, and M. Pernot, in *2015 IEEE International Ultrasonics Symposium (IUS)* (IEEE, 2015), p. 1.
[34]G.-Y. Li, Q. He, G. Xu, L. Jia, J. Luo, and Y. Cao, J. Biomech. **51**, 97 (2017).
[35]A. Wolak, H. Gransar, L. E. J. Thomson, J. D. Friedman, R. Hachamovitch, A. Gutstein, L. J. Shaw, D. Polk, N. D. Wong, and R. Saouaf, JACC: Cardiovasc. Imaging **1**(2), 200 (2008).
[36]K. J. M. Surry, H. J. B. Austin, A. Fenster, and T. M. Peters, Phys. Med. Biol. **49**(24), 5529 (2004).
[37]M. O. Culjat, D. Goldenberg, P. Tewari, and R. S. Singh, Ultrasound Med. Biol. **36**(6), 861 (2010).
[38]J. Fromageau, J.-L. Gennisson, C. Schmitt, R. L. Maurice, R. Mongrain, and G. Cloutier, IEEE Trans. Ultrason., Ferroelectr., Freq. Control **54**(3), 498 (2007).
[39]G. Lamouche, B. F. Kennedy, K. M. Kennedy, C.-E. Bisaillon, A. Curatolo, G. Campbell, V. Pazos, and D. D. Sampson, Biomed. Opt. Express **3**(6), 1381 (2012).
[40]G. Montaldo, M. Tanter, J. Bercoff, N. Benech, and M. Fink, IEEE Trans. Ultrason., Ferroelectr., Freq. Control **56**(3), 489 (2009).
[41]W.-N. Lee, M. Pernot, M. Couade, E. Messas, P. Bruneval, A. Bel, A. A. Hagege, M. Fink, and M. Tanter, IEEE Trans. Med. Imaging **31**(3), 554 (2012).
[42]E. Widman, E. Maksuti, C. Amador, M. W. Urban, K. Caidahl, and M. Larsson, Ultrasound Med. Biol. **42**(10), 2423 (2016).